minerals

MDPI

Article

Incorporation of Zinc Hydroxide Sulphate (ZHS) Nanoplates into Epoxy Resin to Improve Its Corrosion Protection

Fateme Aliahmadi [1], Davod Seifzadeh [1,*], Roghaye Samadianfard [1] and Burak Dikici [2]

[1] Corrosion and Industrial Electrochemistry Research Laboratory, University of Mohaghegh Ardabili, Ardabil P.O. Box 179, Iran
[2] Department of Metallurgical and Materials Engineering, Ataturk University, Erzurum 25240, Turkey
* Correspondence: seifzadeh@uma.ac.ir; Tel.: +98-4533514702; Fax: +98-4533514701

Abstract: Zinc hydroxide sulphate (ZHS) nanoplates were synthesized and then characterized by various methods, including field-emission electron microscopy (FESEM), Fourier-transform infrared spectroscopy (FTIR), X-ray photoelectron microscopy (XPS), thermal gravimetric analysis (TGA), and the Brunauer–Emmett–Teller (BET) theory. Then, the synthesized ZHS nanoplates were incorporated into the epoxy coating on a ST 37 steel alloy. No change in the morphology of the epoxy coating was observed after incorporating 1 wt. % ZHS nanoplates. Uniform distribution of the incorporated ZHS nanoplates inside the epoxy coating was confirmed by transmission electron microscopy (TEM) and energy-dispersive X-ray spectroscopy (EDS). Atomic force microscopy (AFM) images showed that the surface roughness (S_a) of the neat epoxy coating was about 1.1 µm, which was increased to about 2.1 µm by the incorporation of the ZHS nanoplates. The water contact angle on the coating was changed from 82.1 to 90.8° after incorporating the ZHS nanoplates, which may be attributed to the surface roughness. Electrochemical impedance spectroscopy (EIS) experiments showed that the polarization resistance of the epoxy coating in a 3.5 wt. % NaCl solution after 28 days of immersion was about 2.03 MΩ cm^2, and increased to about 9.47 MΩ cm^2 after adding the ZHS nanoplates. In addition, the capacitance of the ZHS-containing epoxy coating after 28 days of immersion in the corrosive solution was about 0.07 $ns^n\Omega^{-1}cm^{-2}$. The obtained value was more than four times lower than the value obtained for the neat epoxy coating (0.32 $ns^n\Omega^{-1}cm^{-2}$). The results of the EIS measurements indicated a significant increase in the corrosion resistance of the epoxy coating after the addition of the ZHS nanoplates. The improvement in the corrosion was explained by the filling of the possible defects and trapping of the aggressive agents by the incorporated ZHS nanoplates. FESEM and EDS analyses at the end of the immersion period confirmed the results of the corrosion tests.

Keywords: corrosion protection; epoxy resin; nanocomposite; zinc hydroxide sulphate; EIS

Citation: Aliahmadi, F.; Seifzadeh, D.; Samadianfard, R.; Dikici, B. Incorporation of Zinc Hydroxide Sulphate (ZHS) Nanoplates into Epoxy Resin to Improve Its Corrosion Protection. *Minerals* **2023**, *13*, 180. https://doi.org/10.3390/min13020180

Academic Editor: Luciana Sciascia

Received: 12 November 2022
Revised: 19 January 2023
Accepted: 23 January 2023
Published: 26 January 2023

1. Introduction

Epoxy resin is widely used to control the corrosion of metals due to significant advantages compared to other options. The corrosion-resistant epoxy resins are generally applied in thicknesses of several tens of micrometres. However, these coatings have a certain degree of porosity and permeability to corrosive agents like any other organic coatings. Therefore, efforts are needed to further improve the corrosion resistance of epoxy resins. Various strategies have been proposed to increase the corrosion resistance of epoxy resins, including chemical composition modification, mixing with other polymers, multilayer coatings, the addition of a corrosion inhibitor, and adding various nanocompounds [1–5].

The use of nanocompounds is perhaps the most popular method to improve the corrosion resistance of epoxy coatings due to their simplicity and effectiveness. In this regard, a significant number of nanocompounds have been examined. For example, the preparation of epoxy nanocomposites containing silica [2,3], graphene oxide [4,6], carbon nanotubes [7,8], iron oxide [9,10], TiO_2 [11,12], Al_2O_3 [13], CeO_2 [14], ZrO_2 [15], halloysite [16], etc. [17–20] have been reported.

The platelet-like nanocompounds are suitable for the preparation of various corrosion-resistant nanocomposites. These nanocompounds, while allowing chemical interactions with the coating matrix, can also store chemical components such as corrosion inhibitors in the space between their plates and release them intelligently if needed. Various nanocompounds have been synthesized, identified, and used to prepare the corrosion-resistant nanocomposites. Montmorillonite (MMT) is a well-known platelet nanocompound and its benefits to the corrosion resistance of organic coatings have been approved [21–23]. Furthermore, layered double hydroxides (LDHs) have gained more attention in recent years. In addition to having other favorable properties of the layered nanocompounds, LDH can improve the corrosion resistance of coatings by trapping corrosive agents such as chloride ions, etc. LDH nanoplates have been suggested as nano-fillers to increase the corrosion resistance of epoxy coatings [24]. As mentioned, one of the distinctive features of the LDH nanoplates is their ability to trap aggressive species, such as chloride ions. Therefore, if, for any reason such as structural defects in the coating, the corrosive solution penetrates the coating matrix, the dispersed LDH nanoplates trap the chloride ions by anion exchange. Due to this exciting feature, LDH nanoplates are used as nano-fillers for metallic [25], sol–gel [26,27], and organic nanocomposites [28,29]. The LDH nanoplates have also been used as nano-fillers to enhance the corrosion resistance of epoxy coatings. For instance, the positive effects of the molybdate-intercalated Ni-Fe-LDH nanoplates on the anti-corrosion properties of the epoxy resin have been discussed by Peng et al. [30]. Enhancement in the corrosion protection of the epoxy resin was attributed to the chloride-ion trapping and simultaneous molybdate-ion release via the anion-exchange mechanism. In another study, Su et al. [24] has examined the corrosion resistance of the epoxy resin before and after the incorporation of Mg-Al-LDH nanosheets (with nitride-ion intercalation). The remarkable improvement in the anti-corrosion properties was also ascribed to the anion-exchange capacity and barrier properties of the LDH nanosheets.

Zinc hydroxide sulphate (ZHS) with the general formula of $xZn(OH)_2 \cdot yZnSO_4 \cdot zH_2O$ is a new class of platelet-like nanocompounds, which can be easily synthesized [31]. Despite the similarity of the structure, LDH is only able to trap anions by ion exchange, while ZHS can trap cations, anions, and water molecules through the chemical-bonding and phase-transition mechanisms. The ZHS can transform into gordaite ($NaZn_4(OH)_6(SO_4)Cl \cdot 6H_2O$) when encountering the corroding NaCl solution through trapping chloride ions, sodium ions, and water. The chlorine ions are trapped through chemical bonding to the crystal framework of the ZHS rather than anion exchange. The connection of the chlorine ions to the crystal lattice of the ZHS induces a negative charge in the structure, which is compensated by the absorption of hydrated sodium ions.

Due to the aforementioned unique features, the effect of the ZHS nanoplates on the corrosion-protection performance of the fluorocarbon coating in a 3.5 wt. % NaCl solution was investigated [31]. The results showed that the dispersed nanoplates increase the corrosion protection ability of the fluorocarbon coating. When the corrosive electrolyte penetrates the coating matrix, it reaches the nanoplate surface, which causes it to function actively. In a way, water molecules along with sodium and chlorine ions are trapped through the phase-transform mechanism, which results in the inhibition of the electrolyte diffusion to the coating–substrate interface. In addition, the swelling of the ZHS nanoplates increases the intraplate spaces, resulting in better corrosion protection.

The potential capabilities of ZHS nanoplates in trapping water, anions, and cations make them preferable over other nanofillers in the preparation of anti-corrosion nanocomposites. In addition, their synthesis is simple, and cheap materials are used. Therefore, the effect of ZHS-nanoplate incorporation on the corrosion resistance of the epoxy coating was studied in this work. For this purpose, the ZHS nanoplates were synthesized and characterized by the FESEM, BET, TGA, and FTIR techniques. Afterwards, the synthesized nanoplates were incorporated into the epoxy resin at the appropriate concentration. The resultant nanocomposite coating was studied from a different point of view by a set of suitable methods including FESEM, TEM, EDS-mapping, AFM, and EIS.

2. Materials and Methods

2.1. Alloy Samples

In this work, ST 37 steel alloy was used as substrate. ST 37 rebar was cut into disc pieces with a diameter of 2 cm and a thickness of 0.5 cm. Next, a copper wire was soldered to the alloy sample. Afterwards, the samples were placed inside a polyester mount. Next, the polyester mount was removed from the steel surface by abrading with SiC sandpaper (no. 100). Then, the successive abrading of the sample with different grids of the SiC sandpaper (no. 400, 800, 1000, and 2000) was continued to mirror-finish surface. In this way, only one face of the disc samples with a total surface area of 3.14 cm^2 remained free for the coating application and then electrochemical examinations. Before coating application, the alloy samples were carefully washed with tap and distilled water, degreased by ethanol in the ultrasonic bath, and finally dried at room temperature.

2.2. Synthesis of the ZHS Nanoplates

The ZHS nanoplates were prepared via the chemical bath deposition technique. For this purpose, two different solutions with a total volume of 200 mL, and a concentration of 0.2 M were prepared by dissolving $ZnSO_4 \cdot 7H_2O$ and hexamethylenetetramine in the deionized water. The prepared solutions were mixed and then 400 mL ethanol was added. Next, several drops of diluted H_2SO_4 solution were added to the mixture to adjust its pH to within the range of 5 to 6. The obtained solution was covered by a nylon film and then heated to 70 °C for 2 h. Then, the solid white product was collected by filtering. Afterwards, the solid product was dried at laboratory temperature after washing with deionized water and ethanol.

2.3. Coating Application

First, the epoxy resin and hardener were added to each other in a ratio of 2:1 and then were mixed at 700 rpm for 10 min to reach a homogenous coating solution. Next, the mixture was applied to the steel specimens using a brush. The samples were held in the laboratory for 24 h. Then, the samples were placed in a digital oven. The oven temperature gradually reached 100 °C with a ramping rate of 5 °C min^{-1}, and the curing treatment was performed for 1 h. At the end, the coated specimens were removed after naturally cooling to room temperature. In order to apply the nanocomposite coating, the ZHS nanoplates were added to the hardener of the epoxy resin. Then, the ZHS-containing hardener solution was intensively agitated for 2 min using an ultrasonic probe. Then, it was placed in an ultrasonic bath for 30 min. The epoxy resin was then added to the hardener/ZHS mixture, and the mixture was stirred for 10 min. The final concentration of the nanoplates in the nanocomposite coating was 1% by weight. After preparation of the ZHS-containing epoxy mixture, it was applied on the ST 37 alloy samples in a similar manner to that which was described above.

2.4. Characterization

2.4.1. ZHS Nanoplates

First, the synthesized ZHS nanoplates were morphologically analyzed by FESEM (MIRA 3, TESCAN). Moreover, the ZHS nanoparticles were also analyzed by XPS (SPECS FlexPS) and FTIR techniques. In addition, the thermal stability and total surface area of the ZHS nanoplates were studied by TGA and BET methods, respectively.

2.4.2. Epoxy Coatings

FESEM method was used to study the surface and cross-section morphologies of the epoxy coating before and after addition of the ZHS nanoplates. Prior to the microscopic analysis, the coated samples were plated with a thin layer of gold due to the inherent low conductivity of the epoxy coating. To prepare the cross-sectional images, the coated samples were cut. Then, the cross-section area of the coated alloy parts was gently abraded with SiC sandpaper (no. 400 to 2000) to capture the microscopic images without creating

an artificial rupture in the metal–coating interface. In addition, EDS-mapping analysis was carried out on the cross-sectional areas in order to confirm the uniform distribution of ZHS nanoplates. Furthermore, to verify uniform distribution of the ZHS nanoplates inside the epoxy resin, a thin layer with a thickness of 50 nm was separated from the surface of the nanocomposite coating and then analyzed by TEM. Additionally, topography and surface roughness of the applied coatings were examined by AFM (CoreAFM, Nanosurf) analysis in an extensive range of 50 × 50 μm^2 using Si_3N_4 cantilever tip.

The effect of ZHS nanoplates on the hydrophobicity of the epoxy coating was evaluated by measuring the contact angle of water droplets on its surface. For this purpose, a drop of water was deposited on five different coating points. Then, the contact angles were calculated by recording the relevant images, and the results were averaged.

Finally, the corrosion protection by the conventional and nanocomposite epoxy coatings were evaluated by performing EIS tests at different immersion times (4–28 days) in 3.5 wt. % NaCl solution. The tests were performed by applying an alternating potential of 20 mV around the open-circuit potential of the samples in the frequency range of 100 kHz to 10 mHz. The corrosion experiments were performed in ambient conditions without agitation, aeration, or deaeration of the corrosive environment. The corrosion tests were repeated four times to obtain average results.

3. Results and Discussion

3.1. Characterization of the ZHS Nanoplates

The FESEM images taken from the synthesized ZHS nanoplates show a hexagonal morphology (Figure 1a–c). The dimensions of the ZHS sheets vary from a few micrometres to tens of micrometres. From the morphological image shown in Figure 1c, it is clear that the thickness of the ZHS nanoplates is much lower than their width.

The ZHS nanoplates were also characterized by FTIR (Figure 2). The broad IR band at 3200–3600 cm^{-1} is related to the O-H stretching of the intra-layer or physically-adsorbed water molecules. In addition, the bands at 1122 and 596 cm^{-1} are attributed to the stretching and bending modes of sulphate ions, while the bands at 1000 and 790 cm^{-1} are more probably related to Zn-OH. Finally, the IR band at around 446 cm^{-1} is related to Zn-O [31].

The survey and high-resolution XPS spectra of the ZHS nanoplates were recorded (Figure 3). The presence of XPS peaks related to the zinc, Sulphur, and oxygen elements in the survey scan indicates the successful synthesis of the ZHS nanoplates [32]. The high-resolution Zn 2p XPS spectrum contains two peaks at 1045.4 and 1022.4 eV for Zn 2p1/2 and Zn 2p3/2, respectively. Two spin energy levels are separated by about 23 eV, which is typical for Zn (II) species. The S2p high-resolution spectrum was deconvoluted in doublets at 167.8 and 168.7 eV for $S2p_{1/2}$ and $S2p_{3/2}$, respectively, which can be attributed to sulphate in the ZHS structure. The high-resolution O 1s peak was deconvoluted to give three peaks, centred at 530.3, 531.7, and 532.3 eV, which correspond to the Zn-O, H-O, and S-O bonds, respectively [33]. It should be noted that a line shape function was used in the *XPS* data analysis by CASA XPS software. The U2 Tougaard model is used for background subtraction. In addition, all the binding energies were calibrated to the carbon, C 1s peak at 285 eV. Full information about the XPS spectrum analyses including uncertainties are given as supplementary material (see Figure S1a–c).

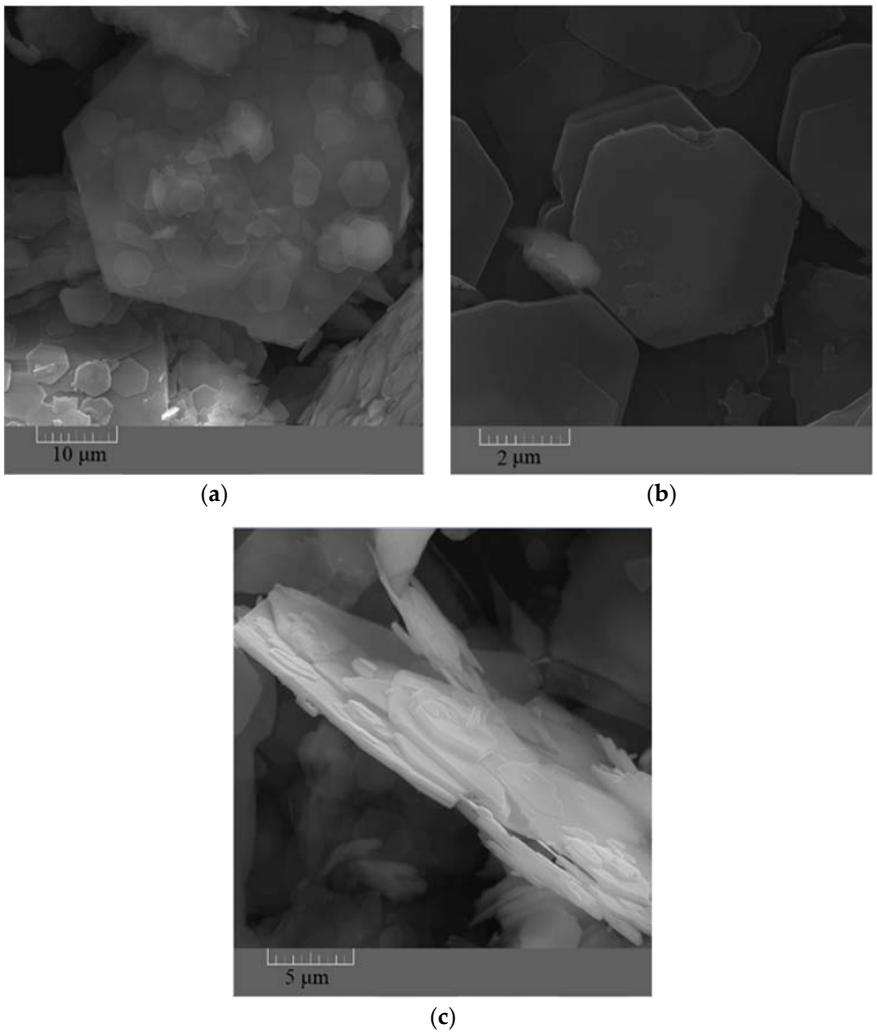

Figure 1. FESEM images showing shape (**a**,**b**) and thickness (**c**) of the synthesized ZHS nanoplates.

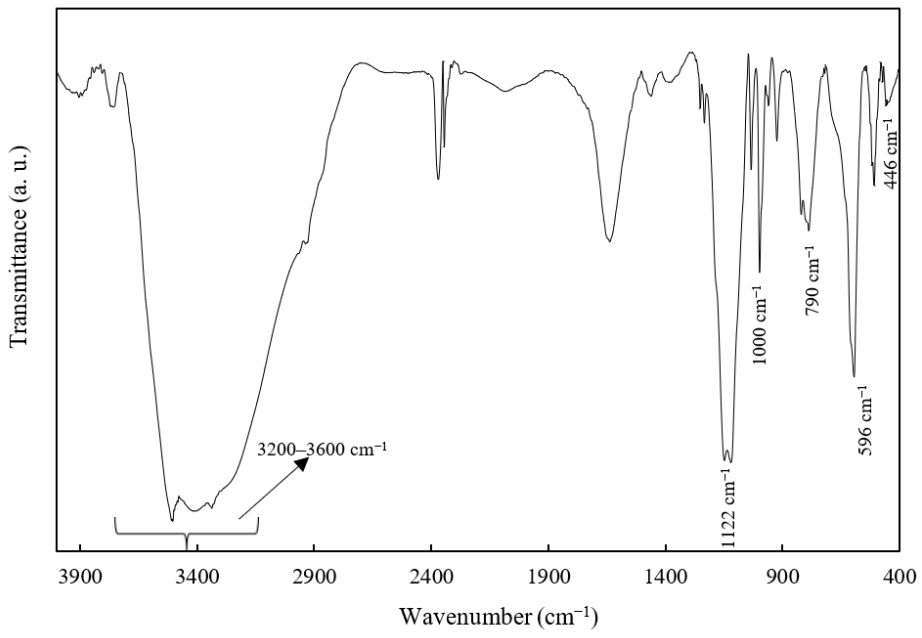

Figure 2. The FTIR spectrum of the as-synthesized ZHS nanoplates.

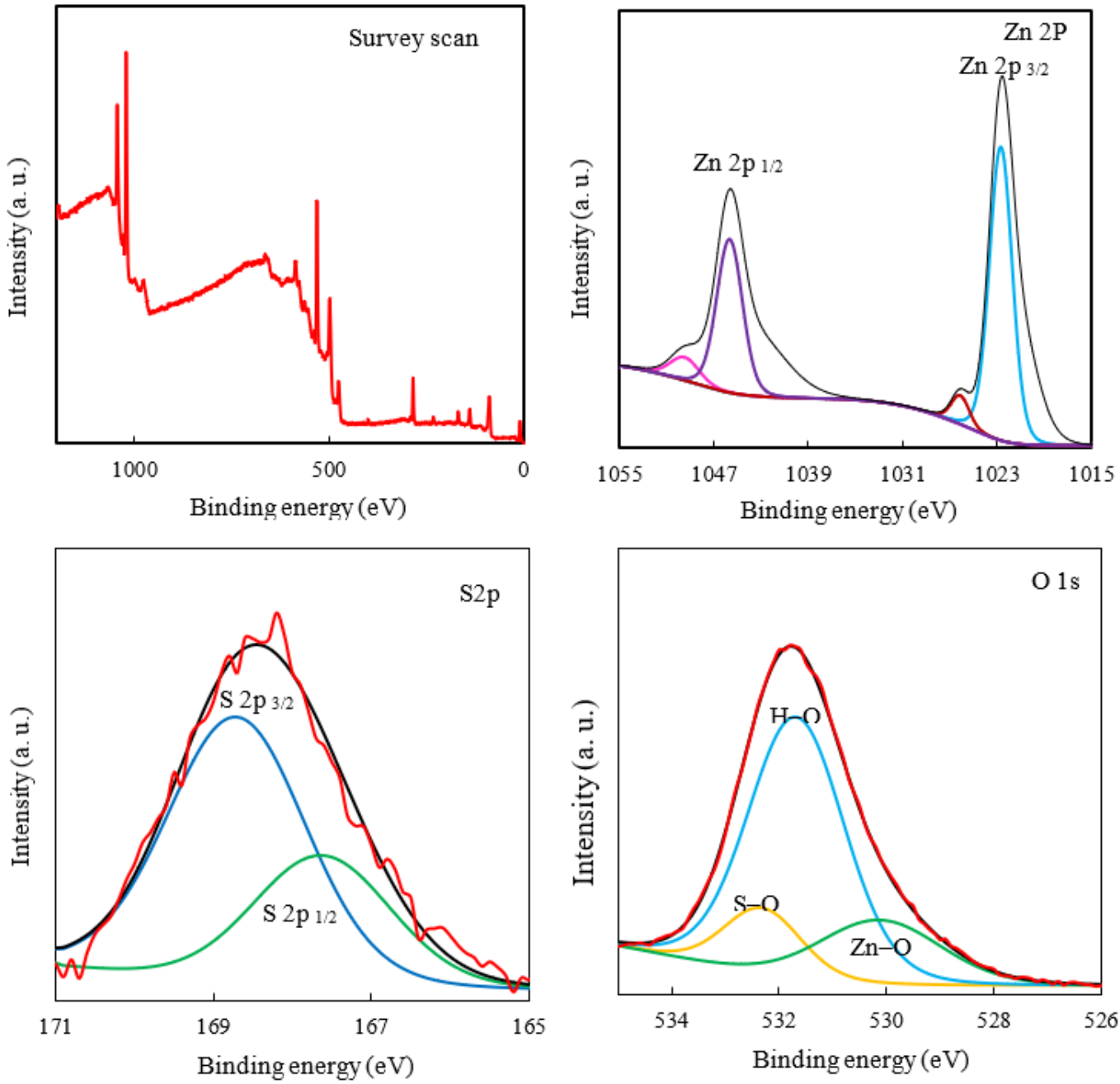

Figure 3. The survey scan and high-resolution XPS spectra of the ZHS nanoplates.

Thermal decomposition of the ZHS nanoplates was also studied in the temperature range of 20 to 700 °C [34]. The recorded TGA curve, along with the results of the quantitative analysis, is given in Figure 4. The thermal decomposition of the ZHS compound includes successive dehydration, dehydroxylation, and SO_2 evolution stages. The dehydration process occurs in the low temperature range and does not modify the layered structure [34]. The release of water from the last hydroxide layer causes it to dehydrate. Therefore, ZnO and $Zn_3(OH)_2(SO_4)_2$ compounds were formed. Decomposition of the $Zn_3(OH)_2(SO_4)_2$ in the second dehydroxylation step leads to the formation of $Zn_3O(SO_4)_2$ in the intermediate temperature range. Decomposition of the sulfates at high temperatures causes SO_2 gas evolution.

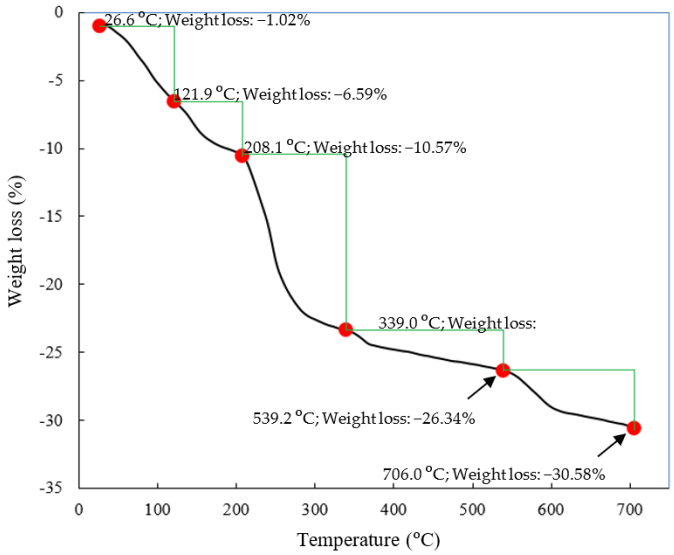

Figure 4. TGA curve of the synthesized ZHS nanoplates.

The nitrogen adsorption–desorption isotherm, along with the BJH plot of the ZHS nanoplates, are given in Figure 5a,b, respectively. The main parameters are specific surface area ($a_{s,BET}$), mean pore diameter (r_p), and the most probable pore size ($r_{p,\ peak}$(area)), and these equal to about 8.72 $m^2\ g^{-1}$, 2.3 nm, and 1.9 nm, respectively. Based on the obtained data, the synthesized nanoplates can be classified as mesoporous compounds.

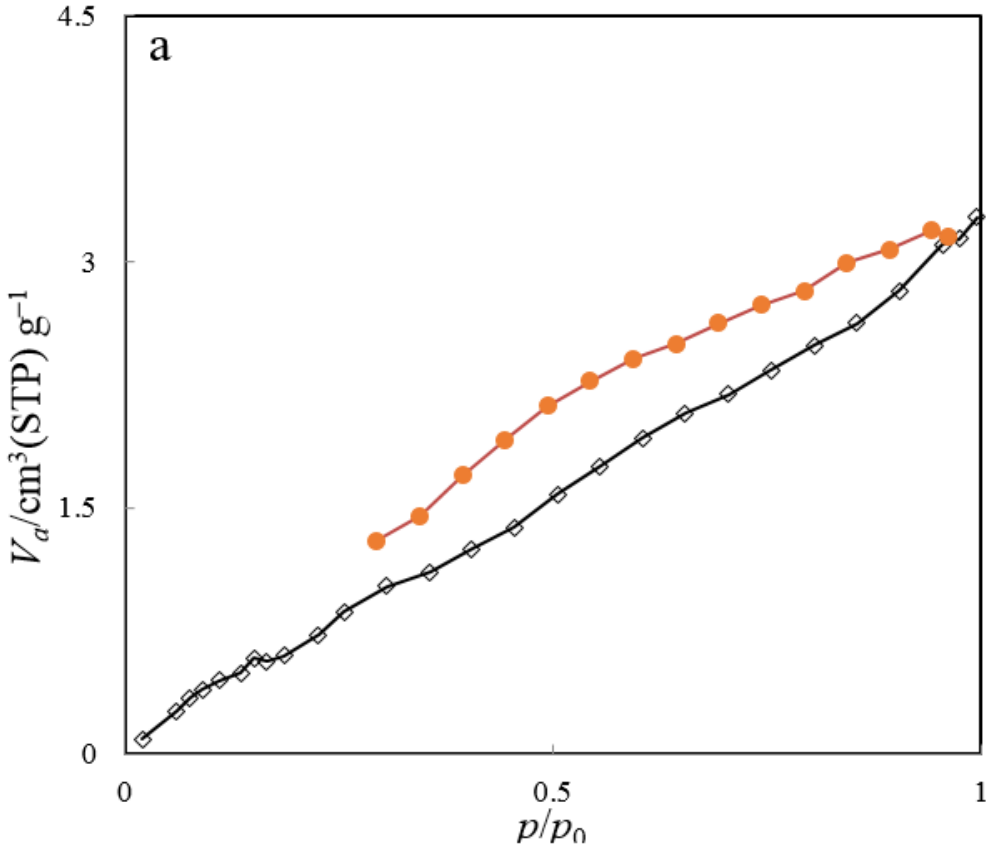

Figure 5. *Cont.*

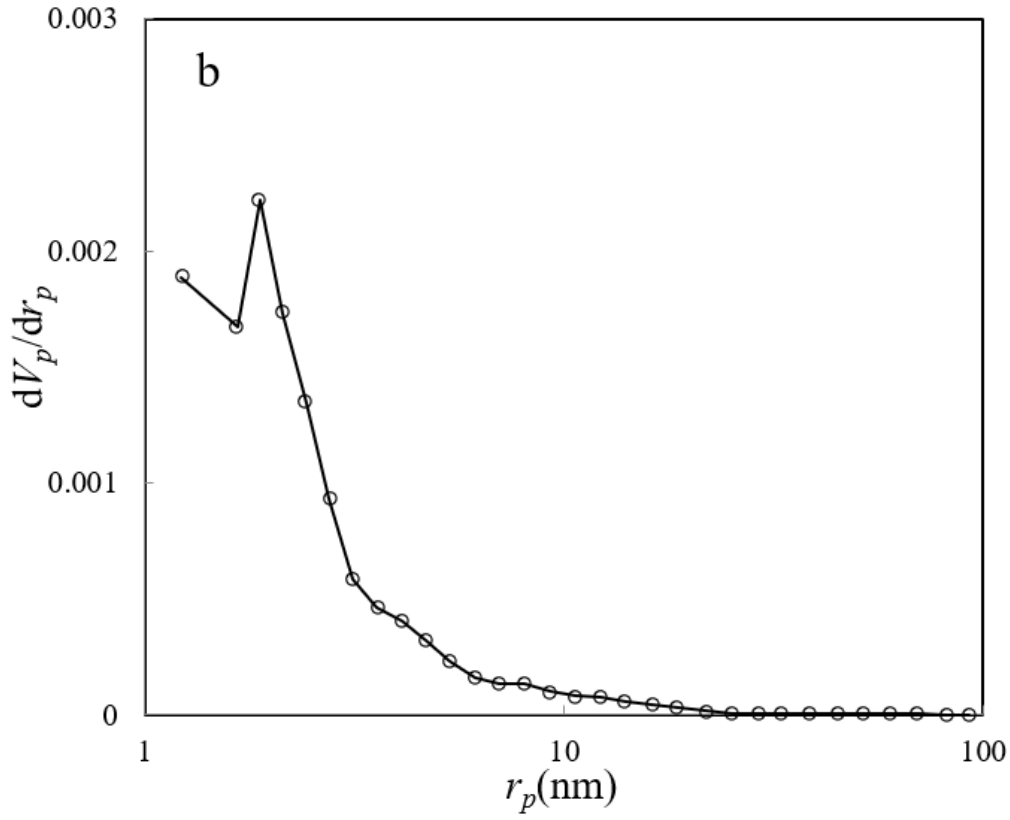

Figure 5. BET nitrogen adsorption–desorption (**a**) and BJH plot (**b**) of the ZHS nanoplates.

3.2. Characterization of the Coatings

3.2.1. Surface Analysis

The images taken with FESEM show that the morphological properties of the epoxy resin at low and high magnifications (Figure 6a,b, respectively) did not change after the addition of the ZHS nanoplates at a 1 wt. % concentration (Figure 6c,d). At low magnification, it can be seen that both neat and nanocomposite epoxy resins are free of large defects. However, the high-magnification image shows the presence of easily-detectable micro-cracks. The cracks and defects have the same pattern for the neat and ZHS-containing epoxy coatings. The formation and propagation of such defects have a detrimental effect on the corrosion resistance of the epoxy resin because they provide easy penetration paths for the corrosive agents toward the metal substrate. Usually, in cases where there is no chemical interaction between the incorporated nanocompounds and the coatings, the addition of the nanocompound has no effect on the size and number of the cracks in the coating. Conversely, the addition of a large amount of the nanocompounds may lead to their aggregation, which has a negative effect on the coating morphology. It seems that such negative effects have not occurred here due to the use of the appropriate concentration of the ZHS nanoplates and their proper dispersion within the coating.

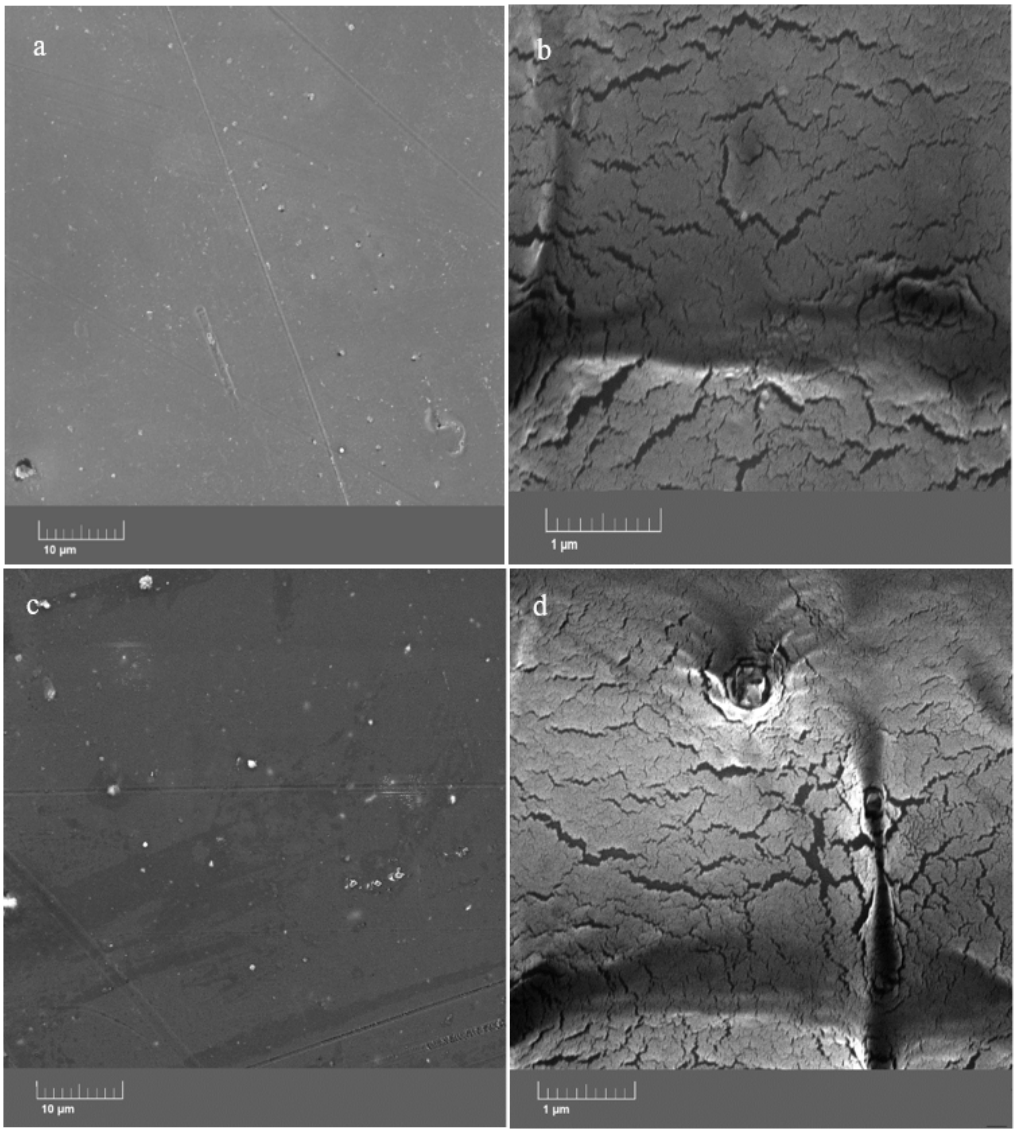

Figure 6. FESEM images of the neat (**a**,**b**) and ZHS-containing (**c**,**d**) epoxy coatings.

To confirm this fact, ultramicrotomy was used for cutting the ZHS-containing resin into extremely thin slices with an approximate thickness of 50 nm. Then, the thin slices were studied by TEM at different magnifications. The presence of the ZHS aggregates of several hundred nanometers is evident in the prepared slice (Figure 7a,b). By carefully examining the dimension of the aggregates, it can be concluded that the ZHS nanoplates have broken and become smaller as a result of the ultrasonic waves because the dimensions of the identified nanoplates are smaller than their dimension in the corresponding FESEM images. Considering the several-micrometres thickness of the epoxy resin, it is not expected that the ZHS agglomerates with dimensions below several hundred nanometers will have a negative impact on the morphology. By looking more closely at the high-magnification image, it can be seen that the ZHS aggregates contain nanoplates of very small dimensions. Therefore, it can be claimed that the TEM images show a suitable distribution of the ZHS nanoplates within the epoxy resin.

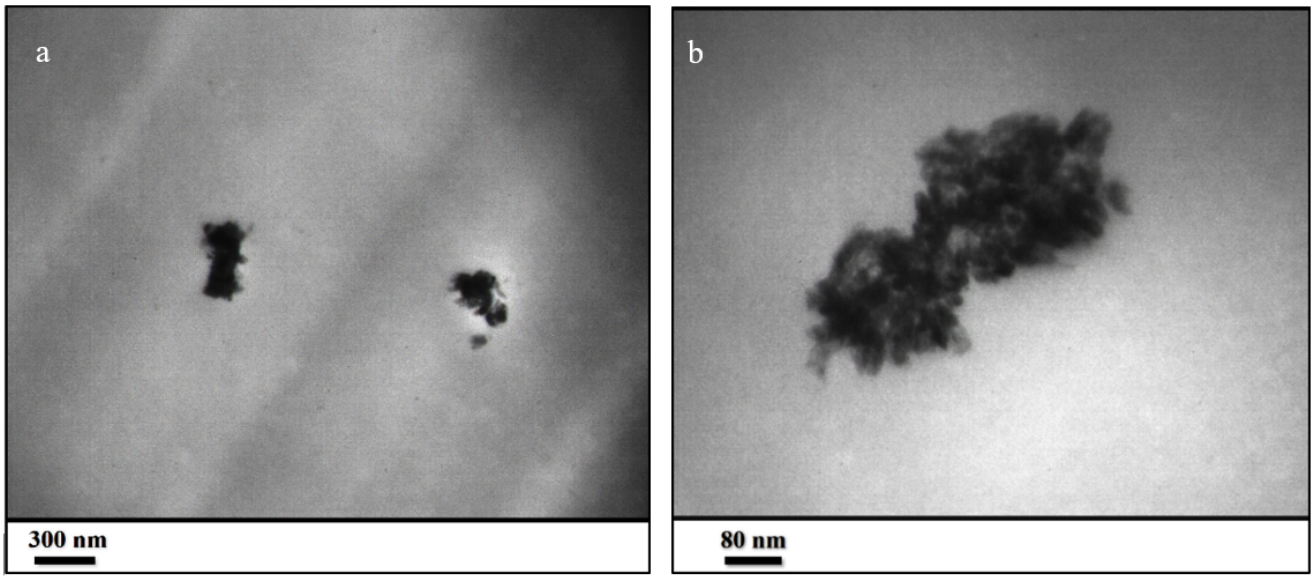

Figure 7. TEM images at low (**a**) and high (**b**) magnifications taken from the thin slice of the ZHS-containing epoxy resin prepared by the ultramicrotomy.

The cross-sectional SEM image (Figure 8a) of the ZHS-containing epoxy resin shows that a uniform coating with an approximate thickness of about 100 μm has been formed on the steel substrate. The same morphology and thickness were observed for the neat epoxy resin which was not reported here to avoid repetition. In general, the matrix of the ZHS-containing epoxy coating is dense. However, some defects are observed, and are characteristic of the epoxy resin. The cross-section area of the ZHS-containing coating was analyzed by EDS. The presence of zinc and sulfur peaks in the EDS spectrum of the coating (Figure 8b) is attributed to the presence of the ZHS nanoplates in the coating. In addition, the corresponding elemental maps clearly show the uniform dispersion of ZHS nanocompounds inside the epoxy resin (Figure 8c–e). Quantitative EDS results were not reported since the accuracy of the analysis for the light atoms (such as carbon and oxygen) is low.

Another essential feature of the coatings is their uniformity, which generally changes after incorporating the nanocompounds. Therefore, the topography of the epoxy resin before and after incorporating the ZHS nanoplates was investigated using the AFM technique (Figure 9a,b, respectively). A change in the topography of the epoxy coating after the addition of the ZHS nanoplates can be easily seen. The surface roughness (S_a) of the neat epoxy coating was about 1.1 μm, and increased to about 2.1 μm after adding the ZHS nanoplates. Increased surface roughness after incorporating the ZHS may be explained by the presence of nanoplates on the surface of the epoxy coating. Usually, at high concentrations of nanocompounds, their aggregation increases, which leads to a decrease in their concentration on the surface of the coating and a decrease in the roughness. In the present study, a relatively low concentration of the ZHS nanoplates was added into the epoxy coating, and as previously shown, aggregation of the incorporated particles was low. Therefore, the surface roughness of the coating has increased due to the dispersion of the nanocompounds in all parts of the coating, including the surface [35].

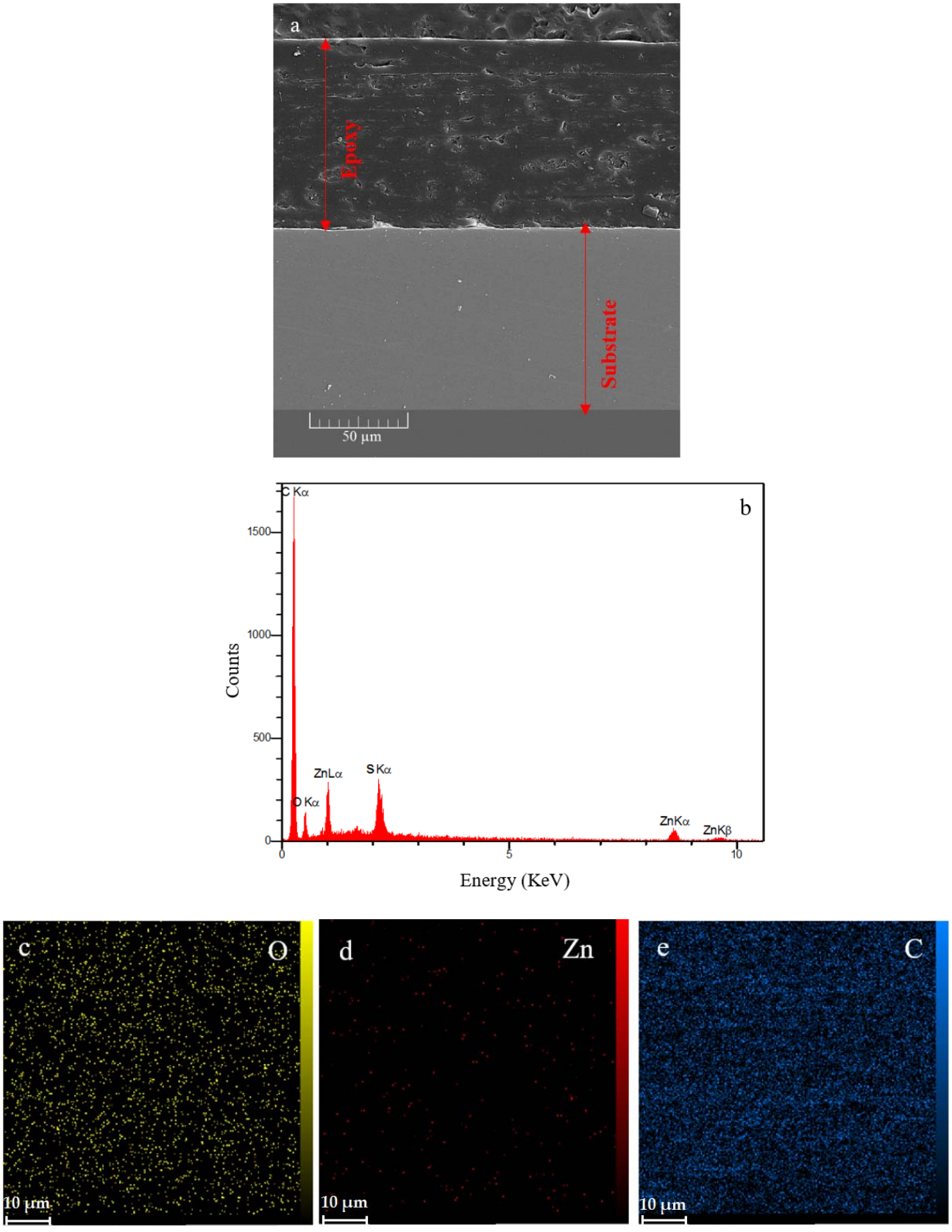

Figure 8. Cross-section area of the ZHS-containing nanocomposite (**a**), together with the corresponding EDS spectrum (**b**) and elemental maps (**c**–**e**).

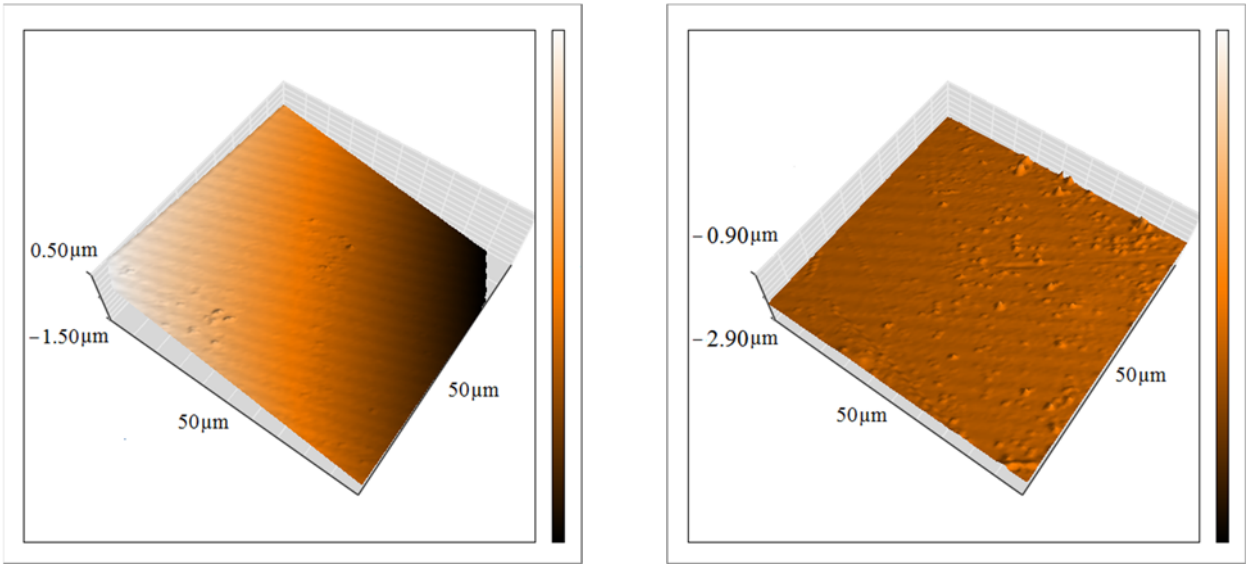

Figure 9. Topography of the neat (**a**) and ZHS-containing (**b**) epoxy coatings obtained by the AFM.

The wettability of the neat and ZHS-containing epoxy coatings was also studied by measuring the static water contact angle on the surface (Figure 10). The average contact angle of the epoxy coating was about 82.1°, and increased to 90.8° after incorporating the ZHS nanoplates. Due to the increase of the contact angle to above 90°, the ZHS-containing epoxy nanocomposite can be classified as a hydrophobic coating [36]. The hydrophobic characteristic of coatings is dependent on the surface. Rough surfaces hold a greater amount of air packets, leading to an increase in the water contact angle. Therefore, the increase in the water on the surface of the epoxy nanocomposite may be related to the increase in the surface roughness after incorporating the ZHS nanoplates, as confirmed by AFM [37]. In addition, the improvement in the hydrophobic properties of the coating can be related to the filling of possible defects with the incorporated nanoplates, which limits water diffusion in the coating.

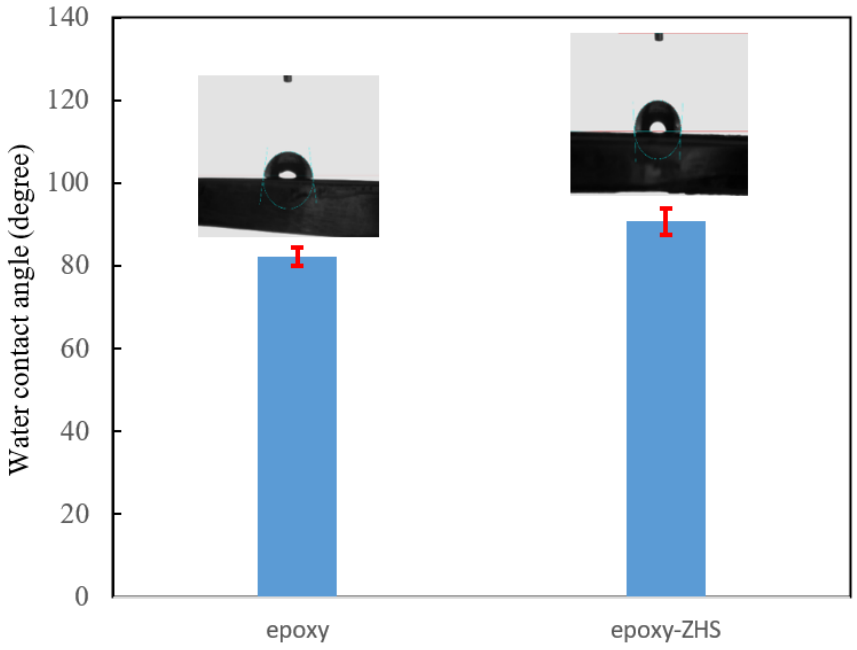

Figure 10. Water contact angle of the neat and ZHS-containing epoxy coatings.

3.2.2. EIS

Finally, the effect of the ZHS-nanoplate incorporation on the corrosion resistance of the epoxy resin was evaluated by EIS. For this purpose, various EIS measurements in a 3.5 wt. % NaCl solution were carried out. Figure 11 shows the typical Nyquist plots for the neat (a) and ZHS-containing (b) epoxy coatings at various immersion times. Corresponding Bode plots were also reported as Supplementary Material (See Figure S2a,b). At high and medium frequencies, a capacitive semicircle is clearly observed in the Nyquist plots. This semicircle is related to the capacitive behavior and resistance of the epoxy coating on the steel alloy. The coating resistance element (R_c) as well as a constant phase element (CPE_c) to account for the non-ideal capacitive behavior of the epoxy coatings can be considered in any equivalent circuit chosen to fit the experimental data. At low frequencies, typical behavior for the finite-length Warburg (FLW) element was observed. Initial evaluations using the zview2 software showed that the fractal FLW element has the best fit with the experimental data at low frequencies. Deviations from the ideal FLW behavior may be attributed to the frequency dispersion on the heterogeneous surface. FLW impedance is typically observed in systems with a one-dimensional diffusion through a finite-length film and fixed activity of the diffusing species. The impedance of the fractal FLW element can be described by the following equation [38,39]:

$$Z_{f.FLW} = \frac{Z_0}{(j\omega\tau_0)^n} \tanh(j\omega\tau_0)^n, n \leq 0.5 \quad (1)$$

where Z_0 represents the Warburg coefficient; in this case, the diffusion resistance at the low-frequency limit. In addition, j, ω, τ_0 are imaginary unit, angular frequency, and characteristic time constant, respectively. The factor n shows the deviation of the FLW element from the ideal state. For n = 0.5, Equation (1) takes the form of the ideal FLW impedance. By considering the fractal FLW element ($W_{f\cdot FLW}$), solution resistance (R_s), R_c, and CPE_c, an appropriate equivalent circuit for the studied coatings was obtained (Figure 11c). The recorded experimental data were fitted using the equivalent circuit and the results were summarized in Table 1. Each experiment was repeated four times, and the quantitative results were averaged. Since the corrosion process show diffusion-controlled kinetics, the polarization resistance (R_p) values in Table 1 have been calculated by summing the coating resistance (R_c) and Z_0. The polarization resistance has an inverse linear relationship with the corrosion rate. Therefore, increasing the polarization resistance of the coating means improving its corrosion resistance [38].

Table 1. EIS parameters of the neat and ZHS-containing epoxy coatings after different immersion times.

Days	Sample	CPEc ($ns^n\Omega^{-1}cm^{-2}$)	n_c	R_c ($M\Omega\ cm^2$)	Z_0 ($M\Omega\ cm^2$)	τ_0 (s)	$n_{f\cdot FLW}$	R_p ($M\Omega\ cm^2$)	Chi-Squared
4	Epoxy	0.56	0.8914	1.25	3.57	99.5	0.327	4.82 ± 3.58	0.0066
	Epoxy-ZHS	0.04	0.9998	0.53	8.33	8.5	0.489	8.86 ± 3.02	0.0136
5	Epoxy	0.27	0.8990	1.67	3.81	56.5	0.349	5.47 ± 4.44	0.0050
	Epoxy-ZHS	0.10	0.9278	0.77	7.25	8.9	0.494	8.02 ± 1.92	0.0047
6	Epoxy	0.24	0.8980	1.56	2.98	43.0	0.333	4.54 ± 4.00	0.0049
	Epoxy-ZHS	0.13	0.9072	0.70	6.25	8.5	0.473	6.96 ± 3.39	0.0076
7	Epoxy	0.28	0.8879	0.80	1.59	41.5	0.341	2.39 ± 1.70	0.0084
	Epoxy-ZHS	0.11	0.9193	0.80	6.62	10.6	0.453	7.42 ± 2.84	0.0091
10	Epoxy	0.23	0.8924	1.09	2.96	15.5	0.372	4.05 ± 4.84	0.0084
	Epoxy-ZHS	0.07	0.9523	0.99	7.40	26.1	0.392	8.39 ± 3.81	0.0126

Table 1. *Cont.*

Days	Sample	CPEc ($ns^n\Omega^{-1}cm^{-2}$)	n_c	R_c ($M\Omega\ cm^2$)	Z_0 ($M\Omega\ cm^2$)	τ_0 (s)	$n_{f\cdot FLW}$	R_p ($M\Omega\ cm^2$)	Chi-Squared
14	Epoxy	0.25	0.8789	0.61	1.88	63.7	0.314	2.48 ± 2.46	0.0053
	Epoxy-ZHS	0.44	0.9134	1.04	6.69	22.9	0.390	7.73 ± 4.50	0.0062
21	Epoxy	0.21	0.8762	0.70	2.14	41.7	0.346	2.84 ± 2.44	0.0147
	Epoxy-ZHS	0.14	0.9199	1.10	10.38	47.8	0.354	11.47 ± 9.33	0.0045
28	Epoxy	0.32	0.8513	0.55	1.49	47.9	0.275	2.03 ± 2.44	0.0100
	Epoxy-ZHS	0.07	0.9027	1.26	8.21	23.1	0.425	9.47 ± 8.83	0.0077

The diffusion resistance (Z_0) value of the epoxy coating containing the ZHS nanoplates is higher than that of the neat coating at all immersion times. This result shows that the presence of ZHS nanoplates prevents the easy diffusion of corrosive agents into the epoxy coating. Since the corrosion process is under the diffusion control, increasing the diffusion resistance means reducing the corrosion rate of the steel after adding the ZHS nanoplates into the epoxy coating.

The polarization resistance of both coatings changed with the immersion time. The change in the polarization resistance is related to several factors such as penetration of the corrosive agents, temporary closing of the pores with the corrosion products, dissolution of the corrosion products, swelling of the coatings due to the accumulation of gases resulting from corrosion, etc. Regardless of the changes in R_p that have occurred over the immersion period, the polarization resistance of the ZHS-containing coating is higher than the neat epoxy coating at all immersion times, especially after 21 and 28 days. As reported in Table 1, the polarization resistance of the epoxy coating at the end of the immersion in a 3.5 wt. % NaCl solution was about 2.03 $M\Omega\ cm^2$, and increased to about 9.47 $M\Omega\ cm^2$ by the incorporation of the ZHS nanoplates. This means that the corrosion resistance of the ZHS-containing epoxy coating is about four times higher than the neat coating. Considering the results obtained in similar studies [40–42], the improvement in the corrosion resistance of the epoxy coating is significant in this study.

Various factors such as penetration of the corrosive species, porosity, accumulation of hydrogen gas bubbles, etc. can change the capacitance of the epoxy coating. However, one of the most important factors affecting the CPE_c value is the amount of water diffused into the coating [43]. The calculated CPE_c value for the ZHS-containing coating is lower than the neat epoxy coating at all immersion times. The dielectric constant of water is high and, therefore, water penetration increases the capacitance of the epoxy coating. Therefore, this result shows an improvement in the barrier properties of the epoxy coating after adding the ZHS nanoplates.

3.2.3. Corrosion Protection Mechanism

The epoxy coatings contain micro-defects produced during the application process. Corrosive electrolyte easily finds the micro-defects to diffuse towards the steel substrate, initiating corrosion. The added ZHS nanoplates have a high surface-to-thickness ratio. Therefore, if located in the defects, they can effectively impede the penetration of the corrosive electrolyte, thereby improving the corrosion resistance. Filling the coating defects creates torturous electrolyte pathways that increase the time it takes for the NaCl solution to reach the steel surface, leading to increased corrosion resistance. In addition, when the corrosive electrolyte penetrates into the ZHS-containing epoxy coating, the partially-hydrated ZHS nanoplates transform into tri-, tetra-, and pentahydrate forms by trapping a part of the penetrated water molecules. In this way, the amount of water that can reach the steel surface is reduced and the corrosion resistance is increased. In addition, the swelling of the ZHS nanoplates via trapping the water molecules further suppresses the penetration of the aggressive electrolyte. The ZHS nanoplates are also able to increase the corrosion resistance of the epoxy coating by trapping the aggressive chloride ions. The chloride-ion

trapping occurs via a stable chemical bonding with the crystal framework of the hydroxide layers, not by simple ion insertion or exchange processes. The chemical bond between the chloride ions and the structural network of the ZHS plates induces a negative charge, which compensates via the absorption of the sodium ions. Since the sodium ions tend to hydrate, a significant amount of water is trapped along with them by the ZHS nanoplates [31].

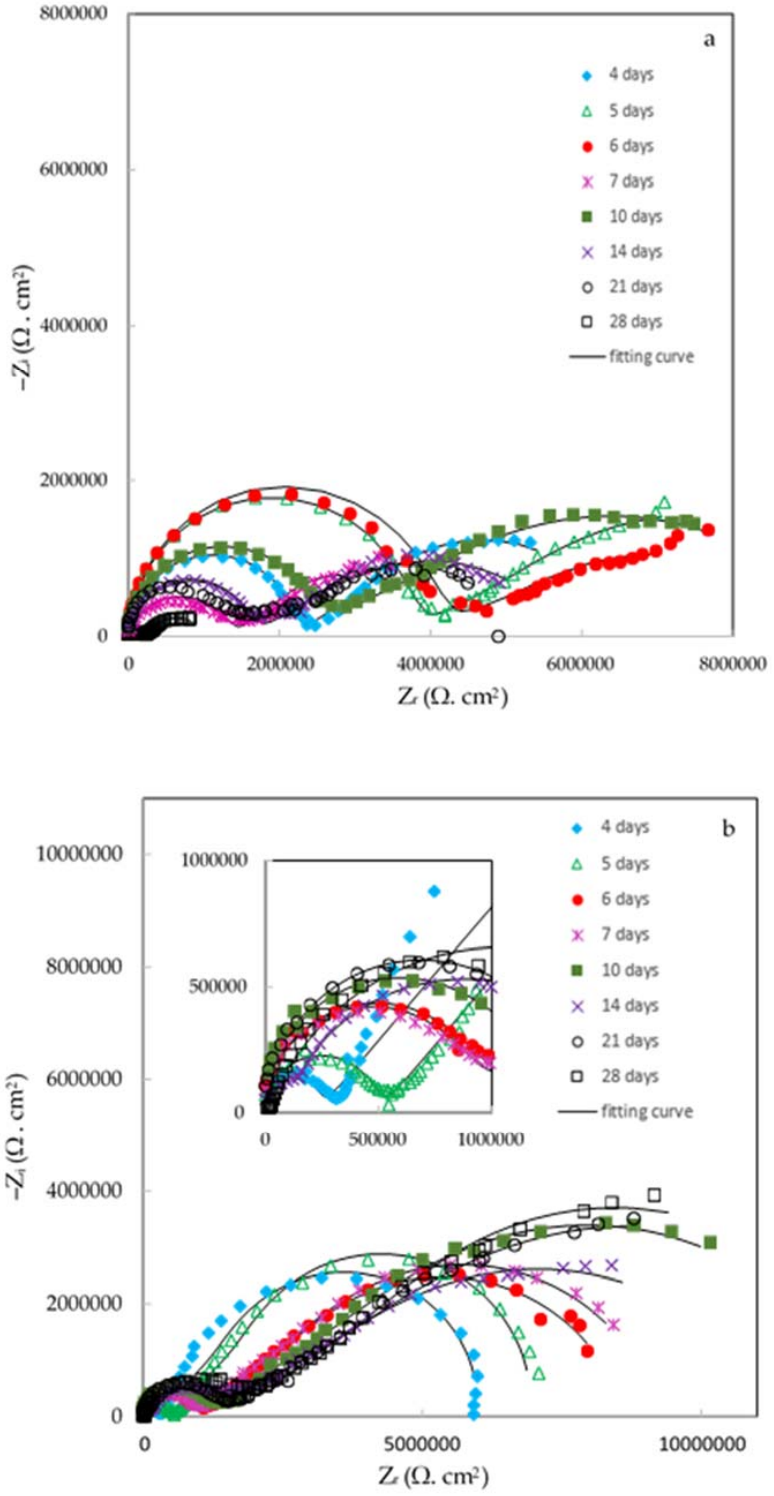

Figure 11. *Cont.*

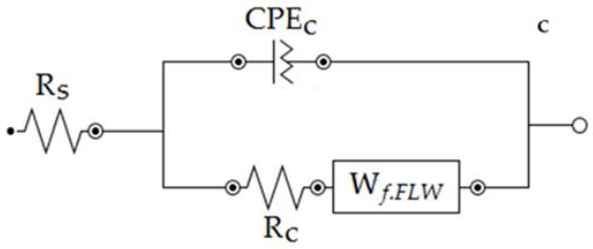

Figure 11. Nyquist plots of the neat (**a**) and ZHS-containing (**b**) epoxy coatings along with the appropriate equivalent circuit (**c**).

3.2.4. Surface Analysis after the Corrosion Tests

The visual images of the neat and ZHS-containing epoxy coatings after 28 days of immersion in the 3.5 wt. % NaCl solution were taken by a digital camera (Figure 12). In each case, three different samples were selected. As it is evident, all the neat epoxy samples were seriously corroded so that severe corrosion damage can be easily observed on the surface. However, the samples containing the ZHS nanoplates remained almost intact after 28 days, and only limited corrosion effects were visible on their surface.

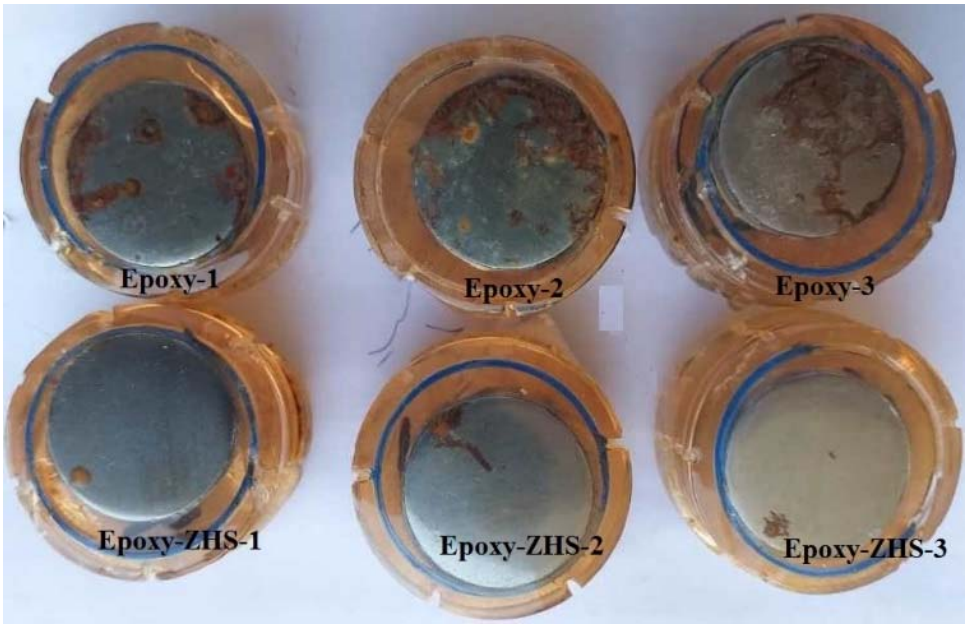

Figure 12. The visual images of the neat and ZHS-containing epoxy coatings after the corrosion tests.

In addition, FESEM and EDS-mapping analyses were performed to study the morphology and chemical composition of the corrosion products, respectively. The parts of the epoxy sample that did not appear to be damaged by the corrosion process were examined at higher magnifications using the FESEM (Figure 13a,b). It is clear that even those parts are seriously damaged by corrosion. The formation of holes with a diameter of several tens of micrometres is obvious. In the high-magnification image (Figure 13b), the formation of crystals, most likely iron oxide/hydroxide, is visible. Corrosion product accumulation was confirmed by examining the elemental map of the affected area. There are large amounts of iron and oxygen as well as chlorine in the damaged area, indicating the formation of iron hydroxide/oxide as well as iron chloride in the damaged area (Figure 13$c_{1–5}$. In addition, the lack of carbon in the mentioned area means that there is no epoxy coating in the damaged area, which is also evident in the relevant microscopic image.

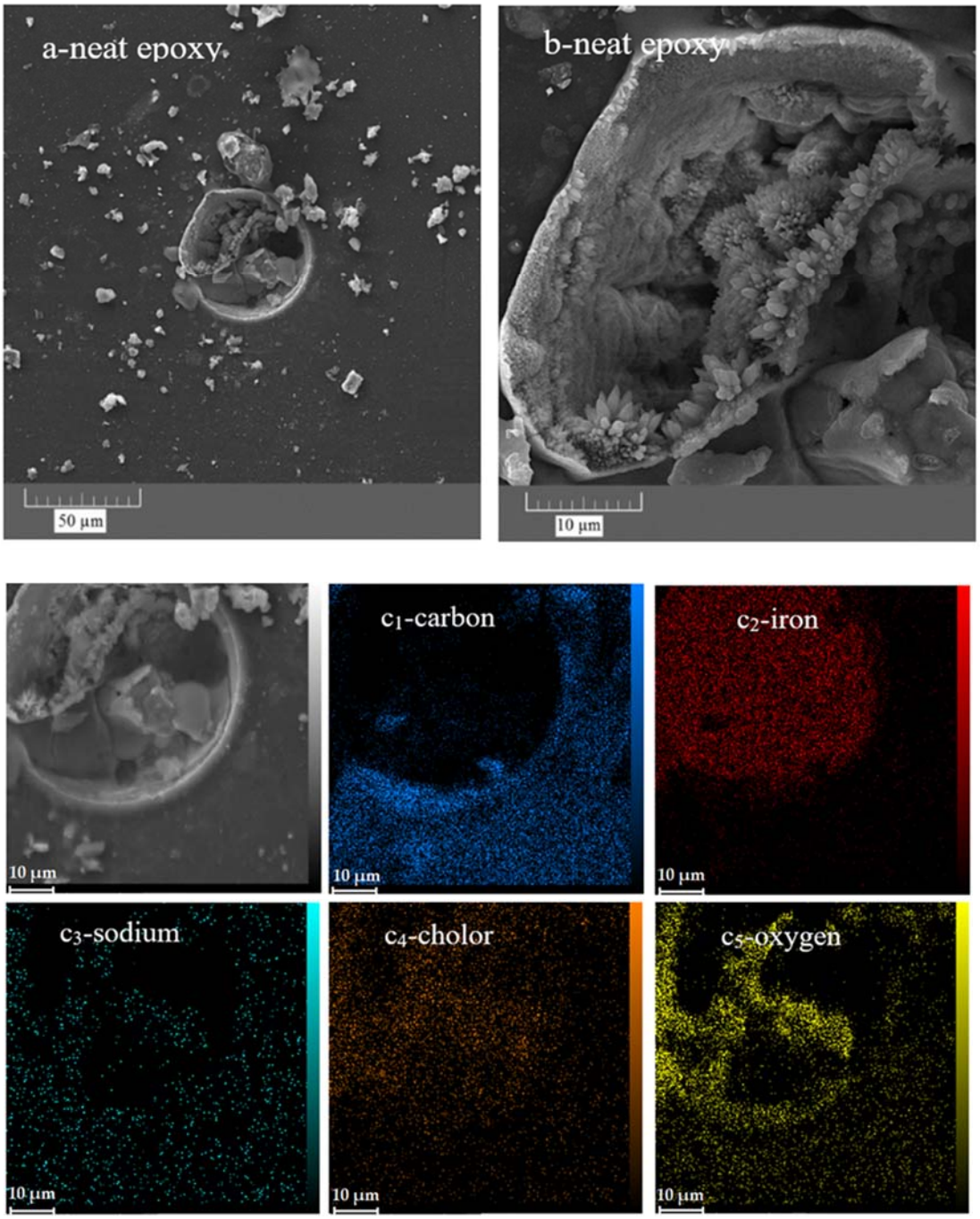

Figure 13. *Cont*.

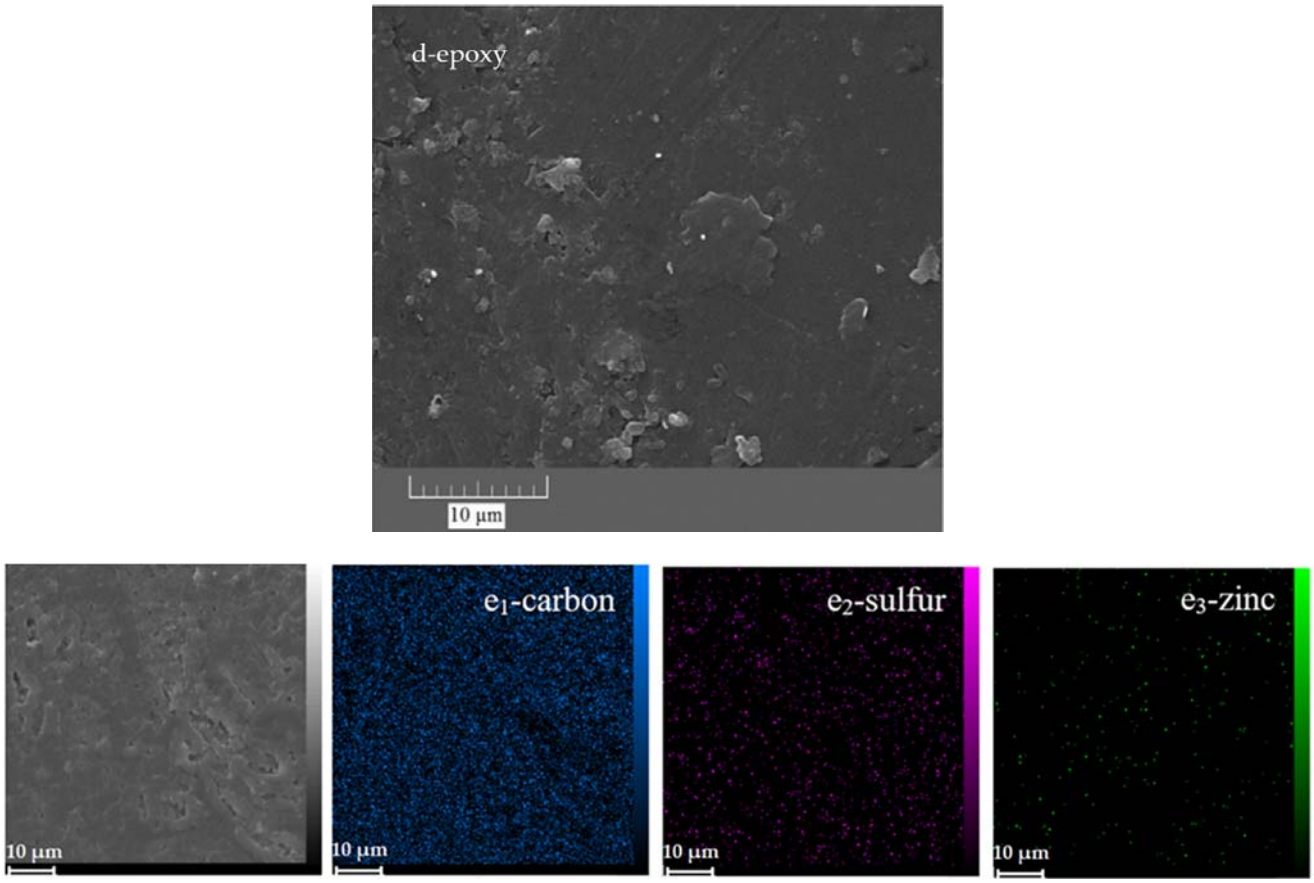

Figure 13. FESEM and EDS-mapping images of the neat (**a**,**b**,**c**$_{1–5}$) and ZHS-containing (**d**,**e**$_{1–3}$) epoxy coatings after corrosion tests.

Conversely, except for areas in the visual image where the accumulation of the iron rust is evident, no corrosion effects were observed in other areas of the ZHS-containing epoxy coating (Figure 13d). Furthermore, high concentrations of iron, oxygen, or chlorine were not observed in the relevant element maps (Figure 13e$_{1–3}$). In addition, low amounts of zinc and sulphur were observed in the prepared maps, which are related to the added ZHS nanoplates. These results, which show the improvement of the corrosion resistance after incorporating the ZHS nanoplates, are in good agreement with the results of the EIS measurements.

4. Conclusions

1. Successful synthesis of the hexagonal ZHS nanoplates with a moderate number of the hydration water was confirmed by FTIR and XPS.
2. The thermal decomposition of the ZHS nanoplates includes successive dehydration, dehydroxylation, and SO_2 evolution.
3. The specific surface area, mean pore diameter, and the most probable pore size of the ZHS nanoplates were 8.72 $m^2\ g^{-1}$, 2.3 nm, and 1.9 nm, respectively.
4. The ZHS nanoplates were uniformly distributed inside the epoxy coating without changing its morphology.
5. The surface roughness of the epoxy coating was increased from about 1.1 to 2.1 µm by the incorporation of the ZHS nanoplates.
6. The water contact angle on the epoxy coating was changed from 82.1 to 90.8° after incorporating the ZHS nanoplates.
7. The results of the EIS measurements indicated a significant increase in the corrosion resistance of the epoxy coating after the addition of the ZHS nanoplates.

Supplementary Materials: The following supporting information can be downloaded at: https://www.mdpi.com/article/10.3390/min13020180/s1, Figure S1: Analysis of the high-resolution XPS peaks: Zn 2p (a), O 1s (b), and Si 2p (c); Figure S2: The Bode plots of the neat (a) and ZHS-containing (b) epoxy coatings after immersion in 3.5 wt. % NaCl solution.

Author Contributions: Conceptualization, D.S. and F.A.; methodology, D.S., F.A., R.S. and B.D.; software, D.S., F.A. and R.S.; validation, D.S., F.A. and R.S.; formal analysis, D.S., F.A. and R.S.; investigation, D.S. and F.A.; resources, D.S., F.A., R.S. and B.D.; data curation, F.A.; writing—original draft preparation, D.S; writing—review and editing, D.S. and B.D.; visualization, D.S. and F.A.; supervision, D.S.; project administration, D.S.; funding acquisition, D.S. All authors have read and agreed to the published version of the manuscript.

Funding: This research received no external funding.

Data Availability Statement: The research data can be provided by the corresponding author's email upon request.

Conflicts of Interest: The authors declare no conflict of interest.

References

1. Song, S.; Yan, H.; Cai, M.; Huang, Y.; Fan, X.; Zhu, M. Multilayer structural epoxy composite coating towards long-term corrosion/wear protection. *Carbon* **2021**, *183*, 42–52. [CrossRef]
2. Xu, Y.; Gao, D.; Dong, Q.; Li, M.; Liu, A.; Wang, X.; Wang, S.; Liu, Q. Anticorrosive behavior of epoxy coating modified with hydrophobic nano-silica on phosphatized carbon steel. *Prog. Org. Coat.* **2021**, *151*, 106051. [CrossRef]
3. Atta, A.M.; Ezzat, A.O.; El-Saeed, A.M.; Tawfeek, A.M.; Sabeela, N.I. Self-healing of chemically bonded hybrid silica/epoxy for steel coating. *Prog. Org. Coat.* **2020**, *141*, 105549. [CrossRef]
4. Zheng, W.; Chen, W.G.; Feng, T.; Li, W.Q.; Liu, X.T.; Dong, L.L.; Fu, Y.Q. Enhancing chloride ion penetration resistance into concrete by using graphene oxide reinforced waterborne epoxy coating. *Prog. Org. Coat.* **2020**, *138*, 105389. [CrossRef]
5. Bagale, U.; Kadi, A.; Potoroko, I.; Rangari, V.; Mahale, M. Ultrasound-assisted Dibutyl phthalate nanocapsules preparation and its application as corrosion inhibition coatings. *Karbala Int. J. Mod. Sci.* **2022**, *8*, 154–168. [CrossRef]
6. Huang, H.; Tian, Y.; Xie, Y.; Mo, R.; Hu, J.; Li, M.; Sheng, X.; Jiang, X.; Zhang, X. Modification of graphene oxide with acrylate phosphorus monomer via thiol-Michael addition click reaction to enhance the anti-corrosive performance of waterborne epoxy coatings. *Prog. Org. Coat.* **2020**, *146*, 105724. [CrossRef]
7. Calheiros Souto, L.F.; Soares, B.G. Polyaniline/carbon nanotube hybrids modified with ionic liquids as anticorrosive additive in epoxy coatings. *Prog. Org. Coat.* **2020**, *143*, 105598. [CrossRef]
8. Deyab, M.A.; Awadallah, A.E. Advanced anticorrosive coatings based on epoxy/functionalized multiwall carbon nanotubes composites. *Prog. Org. Coat.* **2020**, *139*, 105423. [CrossRef]
9. Touazi, Y.; Abdi, A.; Khimeche, K. Influence of heat treatment of iron oxide on its effectiveness as anticorrosion pigment in epoxy based coatings. *Prog. Org. Coat.* **2020**, *139*, 105458. [CrossRef]
10. Jouyandeh, M.; Rahmati, N.; Movahedifar, E.; Hadavand, B.S.; Karami, Z.; Ghaffari, M.; Taheri, P.; Bakhshandeh, E.; Vahab, H.; Ganjali, M.R.; et al. Properties of nano-Fe_3O_4 incorporated epoxy coatings from cure index perspective. *Prog. Org. Coat.* **2019**, *133*, 220–228. [CrossRef]
11. Fadl, A.M.; Abdou, M.I.; Hamza, M.A.; Sadeek, S.A. Corrosion-inhibiting, self-healing, mechanical-resistant, chemically and UV stable PDMAS/TiO_2 epoxy hybrid nanocomposite coating for steel petroleum tanker trucks. *Prog. Org. Coat.* **2020**, *146*, 105715. [CrossRef]
12. Sekhavat, Z.; Ghaemy, P.M.; Bordbar, S.; Karimi-Maleh, H. Effects of surface treatment of TiO_2 nanoparticles on the adhesion and anticorrosion properties of the epoxy coating on mild steel using electrochemical technique. *Prog. Org. Coat.* **2018**, *119*, 99–108. [CrossRef]
13. Wan, P.; Zhao, N.; Qi, F.; Zhang, B.; Xiong, H.; Yuan, H.; Liao, B.; Ouyang, X. Synthesis of PDA-BN@f-Al_2O_3 hybrid for nanocomposite epoxy coating with superior corrosion protective properties. *Prog. Org. Coat.* **2020**, *146*, 105713. [CrossRef]
14. Lei, Y.; Qiu, Z.; Tan, N.; Du, H.; Li, D.; Liu, J.; Liu, T.; Zhang, W.; Chang, X. Polyaniline/CeO_2 nanocomposites as corrosion inhibitors for improving the corrosive performance of epoxy coating on carbon steel in 3.5% NaCl solution. *Prog. Org. Coat.* **2020**, *139*, 105430. [CrossRef]
15. Zivkovic, L.S.; Jegdic, B.V.; Andric, V.; Rhee, K.Y.; Bajat, J.B.; Miskovic-Stankovic, V.B. The effect of ceria and zirconia nanoparticles on the corrosion behaviour of cataphoretic epoxy coatings on AA6060 alloy. *Prog. Org. Coat.* **2019**, *136*, 105219. [CrossRef]
16. Bagale, U.D.; Desale, R.; Sonawane, S.H.; Kulkarni, R.D. An active corrosion inhibition coating of two pack epoxy polyamide system using halloysite nanocontainer. *Prot. Met. Phys. Chem. Surf.* **2018**, *54*, 230–239. [CrossRef]
17. Xia, Z.; Liu, G.; Dong, Y.; Zhang, Y. Anticorrosive epoxy coatings based on polydopamine modified molybdenum disulfide. *Prog. Org. Coat.* **2019**, *133*, 154–160. [CrossRef]

18. Khodaei, P.; Shabani-Nooshabadi, M.; Behpour, M. Epoxy-based nanocomposite coating reinforced by a zeolite complex: Its anticorrosion properties on mild steel in 3.5 wt% NaCl media. *Prog. Org. Coat.* **2019**, *136*, 105254. [CrossRef]
19. Atta, A.M.; El-Faham, A.; Al-Lohedan, H.A.; AL Othman, Z.A.; Abdullah, M.M.S.; Ezzat, A.O. Modified triazine decorated with Fe_3O_4 and Ag/Ag_2O nanoparticles for self-healing of steel epoxy coatings in seawater. *Prog. Org. Coat.* **2018**, *121*, 247–262. [CrossRef]
20. Ammar, S.; Ramesh, K.; Vengadaesvaran, B.; Ramesh, S.; Arof, A.K. Amelioration of anticorrosion and hydrophobic properties of epoxy/PDMS composite coatings containing nano ZnO particles. *Prog. Org. Coat.* **2016**, *92*, 54–65. [CrossRef]
21. Melia, M.A.; Percival, S.J.; Qin, S.; Barrick, E.; Spoerke, E.; Grunlan, J.; Schindelholz, E.J. Influence of clay size on corrosion protection by clay nanocomposite thin films. *Prog. Org. Coat.* **2020**, *140*, 105489. [CrossRef]
22. Olad, A.; Rashidzadeh, A. Preparation and anticorrosive properties of PANI/Na-MMT and PANI/O-MMT nanocomposites. *Prog. Org. Coat.* **2008**, *62*, 293–298. [CrossRef]
23. Truc, T.A.; Thuy, T.T.; Oanh, V.K.; Hang, T.T.X.; Nguyen, A.S.; Causse, N.; Pebere, N. 8-hydroxyquinoline-modified clay incorporated in an epoxy coating for the corrosion protection of carbon steel. *Surf. Interfaces* **2019**, *14*, 26–33. [CrossRef]
24. Su, Y.; Qiu, S.; Yang, D.; Liu, S.; Zhao, H.; Wang, L.; Xue, Q. Active anti-corrosion of epoxy coating by nitrite ions intercalated MgAl LDH. *J. Hazard. Mater.* **2020**, *391*, 122215. [CrossRef] [PubMed]
25. Daugherty, R.E.; Zumbach, M.M.; Sanders, S.F.; Golden, T.D. Design challenges in electrodepositing metal-anionic clay nanocomposites: Synthesis, characterization, and corrosion resistance of nickel-LDH nanocomposite coatings. *Surf. Coat. Tech.* **2018**, *349*, 773–782. [CrossRef]
26. Yasakau, K.A.; Tedim, J.; Zheludkevich, M.L.; Ferreira, M.G.S. Active corrosion protection by nanoparticles and conversion films of layered double hydroxides. *Corrosion* **2014**, *70*, 436–445. [CrossRef]
27. Alibakhshi, E.; Ghasemi, E.; Mahdavian, M.; Ramezanzadeh, B. Fabrication and characterization of layered double hydroxide/silane nanocomposite coatings for protection of mild steel. *J. Taiwan Inst. Chem. E* **2017**, *80*, 924–934. [CrossRef]
28. Tedim, J.; Kuznetsova, A.; Salak, A.N.; Montemor, F.; Snihirova, D.; Pilz, M.; Zheludkevich, M.L.; Ferreira, M.G.S. Zn-Al layered double hydroxides as chloride nanotraps in active protective coatings. *Corros. Sci.* **2012**, *55*, 1–4. [CrossRef]
29. Bouali, A.C.; Serdechnova, M.; Blawert, C.; Tedim, J.; Ferreira, M.G.S.; Zheludkevich, M.L. Layered double hydroxides (LDHs) as functional materials for the corrosion protection of aluminum alloys: A review. *Appl. Mater. Today* **2020**, *21*, 100857. [CrossRef]
30. Peng, G.; Qiao, Q.; Huang, K.; Wu, J.; Wang, Y.; Fu, X.; Zhang, Z.; Fang, T.; Zhang, B.; Huang, Y.; et al. Ni-Fe-MoO_4^{2-} LDHs/epoxy resin varnish: A composite coating on carbon steel for long-time and active corrosion protection. *Prog. Org. Coat.* **2020**, *140*, 105514. [CrossRef]
31. Wang, L.; Wu, W.; Sun, W.; Yang, Z.; Wang, S.; Liu, G. Partially dehydrated zinc hydroxide sulphate nanoplates reinforced coating for corrosion protection. *Chem. Eng. J.* **2019**, *373*, 8–22. [CrossRef]
32. Andreoli, E.; Rooney, D.A.; Redington, W.; Gunning, R.; Breslin, C.B. Electrodeposition of zinc hydroxysulphate nanosheets and reduction to zinc metal microdendrites on polypyrrole films. *J. Nanosci. Nanotechnol.* **2012**, *12*, 338–349. [CrossRef] [PubMed]
33. Liu, X.; Dang, L.; Nai, X.; Dong, Y.; Li, W. Design and preparation of high-aspect-ratio zinc borate whiskers and their effects on mechanical properties of PP nanocomposite. *Res. Chem. Intermed.* **2018**, *44*, 5697–5709. [CrossRef]
34. Staminirova, T.; Petrova, N.; Kirov, G. Thermal decomposition of zinc hydroxy-sulphate-hydrate minerals. *J. Therm. Anal. Calorim.* **2016**, *125*, 85–96. [CrossRef]
35. Hadavand, B.S.; Pishvaei, M.; Hosseininiasari, M. The role of nanoclay on surface roughness and characteristics of epoxypolysulfide nanocomposite. *Prog. Org. Coat.* **2019**, *131*, 60–66. [CrossRef]
36. Ali, F.; Waseem, M.; Khurshid, R.; Afzal, A. TiO_2 reinforced high-performance epoxy-co-polyamide composite coatings. *Prog. Org. Coat.* **2020**, *146*, 105726. [CrossRef]
37. Tran, P.A.; Webster, T.J. Understanding the wetting properties of nanostructured selenium coatings: The role of nanostructured surface roughness and air-pocket formation. *Int. J. Nanomed.* **2013**, *8*, 2001–2009.
38. Arnoult, X.; Arnoult-Ruzickova, M.; Manak, J.; Viani, A.; Brajer, J.; Arrigoni, M.; Kolman, R.; Macck, J. Corrosion and electrochemical properties of Laser-Shock-Peening-Treated stainless steel AISI 304L in VVER primary water environment. *Metals* **2022**, *12*, 1702. [CrossRef]
39. Liu, C.; Bi, Q.; Leyland, A.; Matthews, A. An electrochemical impedance spectroscopy study of the corrosion behaviour of PVD coated steels in 0.5 N NaCl aqueous solution: Part II. EIS interpretation of corrosion behavior. *Corros. Sci.* **2003**, *45*, 1257. [CrossRef]
40. Wang, N.; Cheng, K.; Wu, H.; Wang, C.; Wang, Q.; Wang, F. Effect of nano-sized mesoporous silica MCM-41 and MMT on corrosion properties of epoxy coating. *Prog. Org. Coat.* **2012**, *75*, 386. [CrossRef]
41. Mohammadi, I.; Izadi, M.; Shahrabi, T.; Fathi, D.; Fateh, A. Enhanced epoxy coating based on cerium loaded Na-montmorillonite as active anti-corrosive nanoreservoirs for corrosion protection of mild steel: Synthesis, characterization, and electrochemical behavior. *Prog. Org. Coat.* **2019**, *131*, 119. [CrossRef]

42. Navarchian, A.H.; Joulazadeh, M.; Karimi, F. Investigation of corrosion protection performance of epoxy coatingsmodified by polyaniline/clay nanocomposites on steel surfaces. *Prog. Org. Coat.* **2014**, *77*, 347. [CrossRef]
43. Akbarzadeh, S.; Naderi, R.; Mahdavian, M. Fabrication of a highly protective silane composite coating with limited water uptake utilizing functionalized carbon nano-tubes. *Compos. Part B—Eng.* **2019**, *175*, 10109. [CrossRef]